Jpn. J. Appl. Phys. Vol. 36 (1997) pp. 2874–2882
Part 1, No. 5A, May 1997

Two-Dimensional Fluid Simulation of Capacitively Coupled RF Electronegative Plasmas

Tae Hun CHUNG, Lin MENG*, Hyun Jin YOON and Jae Koo LEE[1]

Department of Physics, Dong-A University, Pusan 604-714, Korea
[1]*Department of Physics, The Pohang University of Science and Technology, Pohang 790-784, Korea*

(Received September 24, 1996; accepted for publication January 20, 1997)

A two-dimensional self-consistent fluid simulation of capacitively coupled rf glow discharges of electronegative plasma with a cylindrically symmetric parallel plate electrode is presented. The model equations include continuity equations, a Poisson equation, and an electron energy balance equation. The two-dimensional distributions of charged particle densities, electric potential, electron temperature, and ionization rate are calculated. The effects of the applied rf voltage, the driver frequency, and the gas pressure on the discharge characteristics are investigated in detail.

KEYWORDS: parallel-plate rf discharge, capacitively coupled discharge, chlorine, electronegative plasma, two-dimensional fluid simulation

1. Introduction

Glow discharges are widely used in a number of applications such as gas discharge lasers, plasma display pannels, relatively high power switches, and plasma processing.[1)] Understanding how and where plasma is created and identifying creation, loss, and transport mechanisms for various species in the plasma are crucial in the design and operation of the plasma sources.

Electronegative gases such as chlorine and chlorine-containing mixtures are used for etching of polysilicon, silicon oxide, and aluminium. The behavior of the charged particle species determines both the physical and the chemical features of the plasma such as the rf power dissipation, the structure of the plasma sheath, and the fluxes of reactive molecules reaching the surface.

Continuum (fluid) models of charged particle distribution appear to be useful in the effort to understand the physical structure of the discharge. Boeuf and Pitchford[2–4)] studied both a helium discharge and a model electronegative discharge. They used the local field equilibrium approximation (LFA) omitting the electron energy equation. The charged particle fluxes consist of a term representing drift due to the electric field and a diffusion term. This model (sometimes called the single-moment fluid model) includes continuity equations for electrons and ions and Poisson's equation for the electric field. Tsai and Wu performed two-dimensional simulations of rf glow discharges in N_2 and SF_6[5)] based on this model. Their results were displayed in the form of the spatiotemporal contours in a cylindrically symmetric geometry. Fluid simulations including an energy balance equation have been performed in one-dimensional space[6–10)] and in two-dimensional space.[11)] However, in the latter, the energy loss of electrons due to exciting collision, which can be a more important energy loss mechanism than the ionization at the relevant electron temperature, was not considered.

In this report, we present a numerical description of rf discharges based on a two-dimensional (2-D) fluid model including an electron energy equation in which various electron energy loss mechanisms can be considered. The outputs such as the spatial distributions of the ionization rate, charged particle density, potential (electric field), and electron temperature are shown on a video monitor screen with 2- or 3-dimensional graphics interactively using Xgrafix.[12)] A two-dimensional simulation can account for the density profiles in the radial direction (or the radial fluxes) and the uniformity of the ion fluxes toward the rf electrode (or substrate). The latter is investigated in depth elsewhere.[13)]

The main purpose of this work is to study some general features of rf discharges, and to analyze the influence of operating parameters (neutral gas pressure, driver frequency, applied rf voltage) on the characteristics of the rf discharge. This report is organized as follows: in §2 a physical model and basic equations are presented, in §3 the calculation are described and discussed , and in section IV conclusions are summarized.

2. Physical Model and Basic Equations

For simplification of the problem, the following assumptions are made: (1) the electron energy distribution is Maxwellian, (2) the particle motion is collision-dominated, and as a result, a fluid model is applicable, (3) the transport parameters, such as mobility and diffusion coefficients of charged particles, are constant, (4) the ionization rate for discharge is a function of electron temperature, (5) the density and temperature of the neutral gas are constant in the chamber, (6) only the ionization and excitation reactions are considered.

At low pressure, the dissociation degree in the discharge is low and the plasma composition can be expected to be simple, with cl_2 the dominant neutral species, cl^- the dominant negative ion, and cl_2^+ the dominant positive ion. For simplicity, we consider representative reactions between these species only. Under these assumptions the model equations are written as[7,8)]

$$\frac{\partial n_e}{\partial t} + \nabla \cdot \boldsymbol{\Gamma}_e = R_i - R_a \tag{1}$$

$$\frac{\partial n_p}{\partial t} + \nabla \cdot \boldsymbol{\Gamma}_p = R_i - R_v \tag{2}$$

*Permanent address: High Energy Electronics Institute, University of Electronic Science and Technology of China, Chengdu, Sichuan 610054, P. R. China.

$$\frac{\partial n_n}{\partial t} + \nabla \cdot \boldsymbol{\Gamma}_n = R_a - R_v \quad (3)$$

$$\frac{\partial}{\partial t}\left(\frac{3}{2} n_e k T_e\right) + \nabla \cdot \boldsymbol{q}_e + e\boldsymbol{\Gamma}_e \cdot \boldsymbol{E} + \sum_l H_l R_l = 0 \quad (l=i, ex) \quad (4)$$

$$\nabla^2 V = \frac{e}{\epsilon_0}(n_e + n_n - n_p) \quad (5)$$

Instead of solving the momentum balance equation, the drift-diffusion approximation is used for the particle fluxes.

$$\boldsymbol{\Gamma}_e = -D_e \nabla n_e - n_e \mu_e \boldsymbol{E} \quad (6)$$

$$\boldsymbol{\Gamma}_p = -D_p \nabla n_p + n_p \mu_p \boldsymbol{E} \quad (7)$$

$$\boldsymbol{\Gamma}_n = -D_n \nabla n_n - n_n \mu_n \boldsymbol{E} \quad (8)$$

$$\boldsymbol{q}_e = -\frac{5}{2} n_e D_e \nabla(kT_e) + \frac{5}{2} kT_e \boldsymbol{\Gamma}_e \quad (9)$$

Here, $n_{e(p,n)}$, $D_{e(p,n)}$, $\mu_{e(p,n)}$ are the density, diffusion coefficient and mobility of electrons (positive ions, negative ions); and V, T_e, k, e, and ϵ_0 are potential, electron temperature, Boltzmann constant, electron charge and permittivity of free space, respectively. H_l is the electron energy loss per collision.

The ionization, attachment, recombination, and excitation rate terms, R_i , R_a, R_v, and R_{ex}, are written in the forms

$$R_i = k_i n_e N \quad (10)$$

$$R_a = k_a n_e N \quad (11)$$

$$R_v = k_v n_p n_n \quad (12)$$

$$R_{ex} = k_{ex} n_e N, \quad (13)$$

where N is the density of neutral gas, and the reaction-rate coefficients, k_i, k_a, k_v, and k_{ex} are described by mathematical fits to the Boltzmann-solution results. They are written as a function of the electron temperature in Arrhenius form,[14]

$$k = AT_e^B \exp\left(\frac{-C}{T_e}\right). \quad (14)$$

Chlorine gas is chosen as a working gas. The basic operating conditions are p = 0.05–0.5 Torr, V_{rf} = 100–200 V, initial charged particle density of $10^9\, cm^{-3}$, and a time step Δt of 10^{-12} s. The chamber to be studied here is a cylindrically symmetric volume confined by two large parallel plates (electrodes) with a separation L and a radial dielectric wall with radius R.

The radius of the electrodes is larger than that of the dielectric wall.[15] The left electrode ($x = 0$) is grounded, while $V = V_{rf} \sin(2\pi f t)$ is applied to the right electrode ($x = L$). Due to the cylindrically symmetric geometry, the simulation can be carried out with a two-dimensional (r, x) system. The boundary conditions for solution of the above equations are as follows: the potentials on the dielectric wall increase from cathode to anode linearly;[3] the densities of charged particles on the electrodes and wall are set to 0; the electron temperature on the electrodes and wall is s assumed to be 1.0 eV since it is difficult to specify,[9] and the secondary electron emission coefficient is 0.07.

The charged particle flux and flux of electron energy are obtained using an exponential scheme.[16] The equations are discretized by the finite difference method for the spatial derivatives, while the time derivatives are discretized by forward Euler differencing (FTCS). The numerical method is described in detail in ref. 13 and 17.

3. Results

On a dedicated Pentium/133 with LINUX, a typical simulation takes 1–2 days. Sampling time is defined as $T_n = n(0.25T)$, where T is the duration of one cycle and $n = 0, 1, 2, 3$.

Figure 1 shows the 2D distributions of the ionization rate, electron temperature, potential, electron density, negative ion density, and positive ion density at T_3. Although the profiles at T_0, T_1, T_2 are not shown, the charged particle and electron densities are not modulated significantly with the sampling time when the steady state is reached. Since in this simulation symmetric parallel plate geometry is used and the dc bias voltage is zero, this results in a symmetric discharge in the axial direction, as can be observed in Fig. 1. The electron temperature has a spatially uniform distribution in the bulk region, and almost symmetric in both sheaths. It is further observed that the charged particle density is rather uniform in the radial direction. The electron density starts to decrease near the radial sheath, whereas the ion (negative and positive) density has a smooth peak near the radial sheath. In the bulk region quasineutrality exists.

In this study, the effect of the operating parameters such as the gas pressure, the applied rf voltage, and the rf frequency were mainly investigated. Since the 2D temperature distribution has a similar profile to that of the ionization rate, the time variations of the ionization rate and potential are shown in detail in the following figures (Figs. 2–4). The ionization profile is the result of the combined effect of the electron density and the electron temperature (mean energy).

Table I. Values of parameters.

	Symbol (unit)	Value
Gas pressure	p (Torr)	0.05–0.5
Gap distance	L (cm)	3.0
Electrode radius	R (cm)	4.0
rf frequency	f (MHz)	10
Secondary electron emission coefficient	γ	0.07
Peak rf voltage	V_{rf} (V)	100–200
Electron diffusivity	D_eN (cm s^{-1})	3.21×10^{22}
Positive ion diffusivity	D_pN (cm s^{-1})	0.395×10^{18}
Negative ion diffusivity	D_nN (cm s^{-1})	0.489×10^{18}
Electron mobility	μ_eN (V cm s^{-1})	6.42×10^{21}
Positive ion mobility	μ_pN (V cm s^{-1})	1.52×10^{19}
Negative ion mobility	μ_nN (V cm s^{-1})	1.88×10^{19}
Neutral gas temperature	T (K)	300

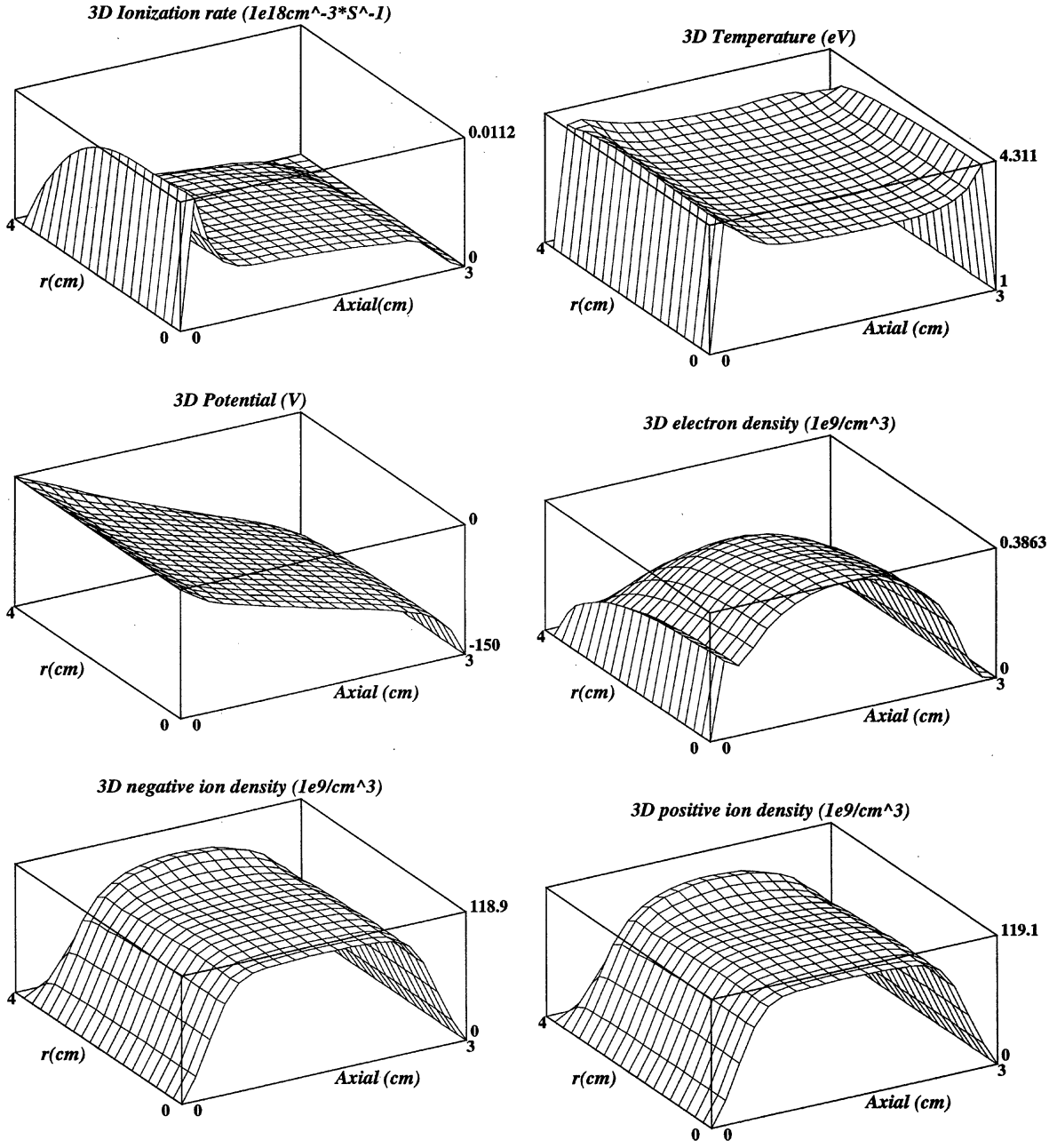

Fig. 1. The profiles of ionization rate, electron temperature, potential, electron density, negative ion density, and positive ion density at T_3 where $V_{rf} = 150\,V$, $p = 0.7\,Torr$, $f = 10\,MHz$.

For the $V_{rf} = 100\,V$ case as shown in Fig. 2, the potential drop across the bulk plasma is significant. The bulk plasma is no longer a nearly equipotential volume. Since the electron density is low, the plasma resistance is correspondingly high. This accounts for the large potential drop.[8] The ionization rate is higher in the radially central region than the sheath region. As for the electric field structure (not shown in the figure), the radial electric field is insignificant compared to that in the electropositive case.

As shown in Fig. 3, when the gas pressure is decreased from 0.5 Torr to 0.05 Torr with other parameters unchanged, the plasma potential increases approximately by more than two-fold, and the potential across the bulk becomes flatter. The ionization rate becomes to have a radially flat distribution (axially, its peak alternates). We also observe that the electron temperature loses its symmetry about the mid-plane.

Figure 4 shows the case in which the rf voltage is 200 V. The potential drop in the bulk is insignificant in this case. The spatial distribution of the electron temperature (not shown) has two axial peaks near the plasma-sheath boundary, and a peak near the radial sheath. The charged particle density profiles exhibit nonuniform distribution along the radial direction. As for the ionization rate profile, the peak occurs in the radial sheath region, and the two axial sheaths have the peak alternately. In contrast to the that in $V_{rf} = 100\,V$ case, this profile shows a strong asymmetry. The peak near the radial sheath is caused by the higher electric field strenth and the higher electron fluxes near the radial wall. This feature is in agreement with other simulation results.[15] One thing to

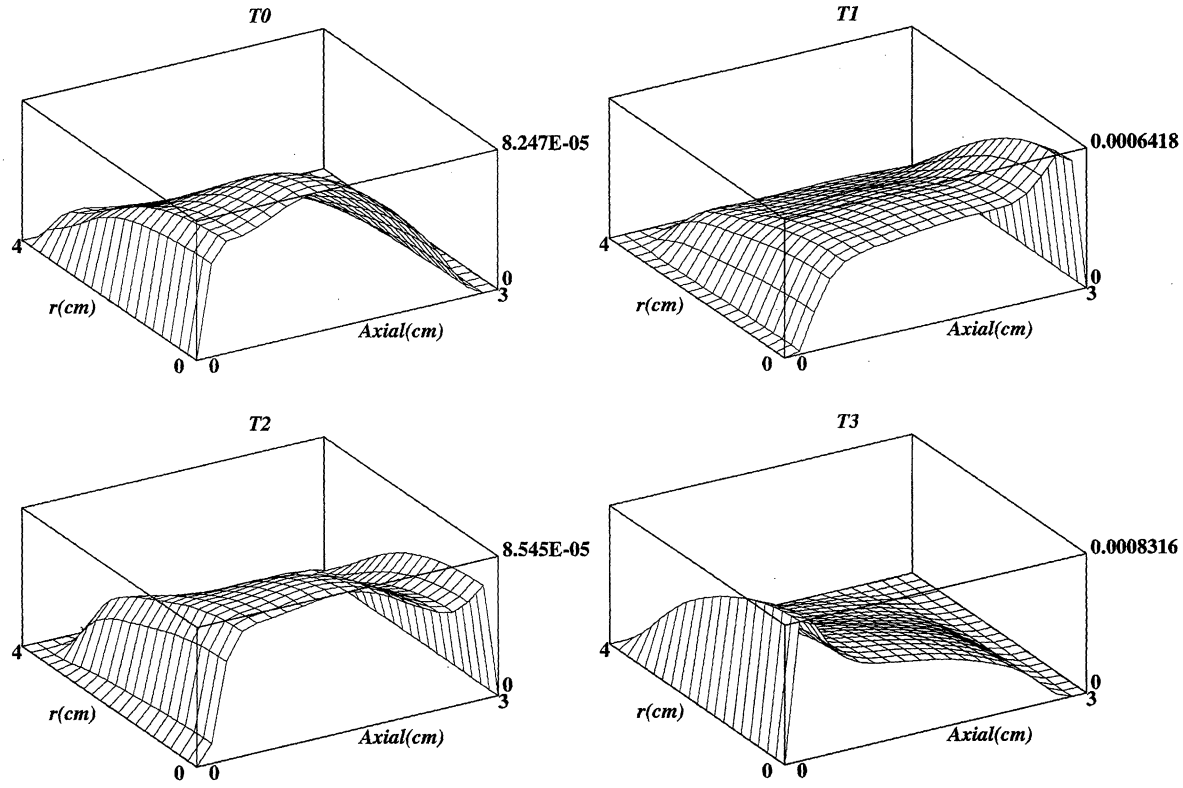

(a)

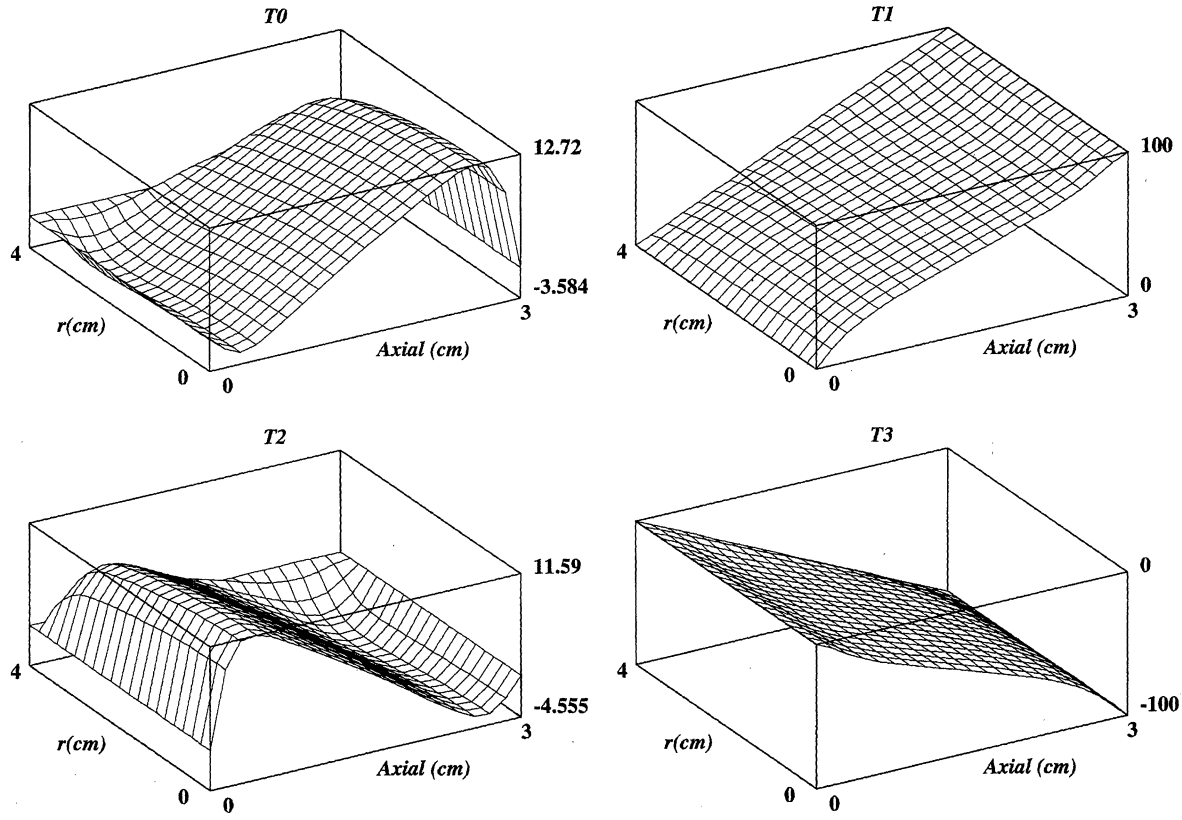

(b)

Fig. 2. (a) Ionization rate (10^{18}/cm^3 s) and (b) potential (V) profiles at four different times of an rf cycle. $V_{rf} = 100$ V, $f = 10$ MHz, $p = 0.5$ Torr.

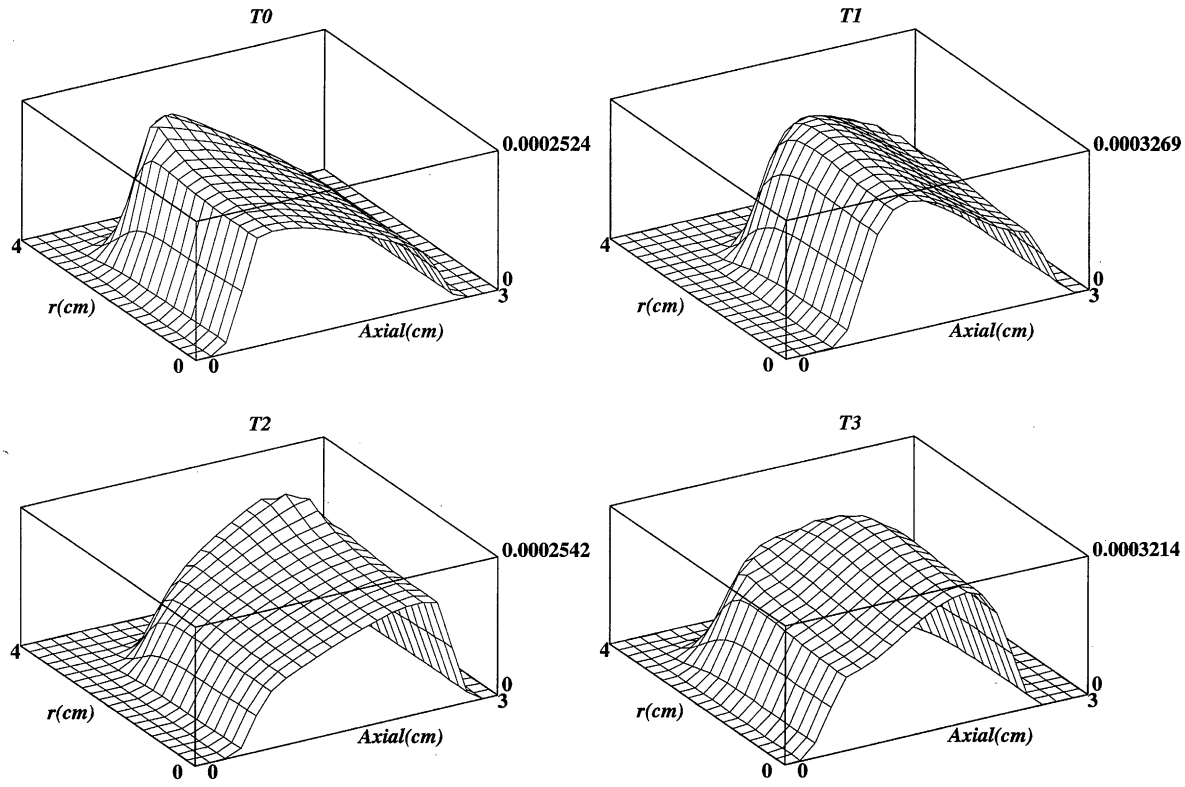

(a)

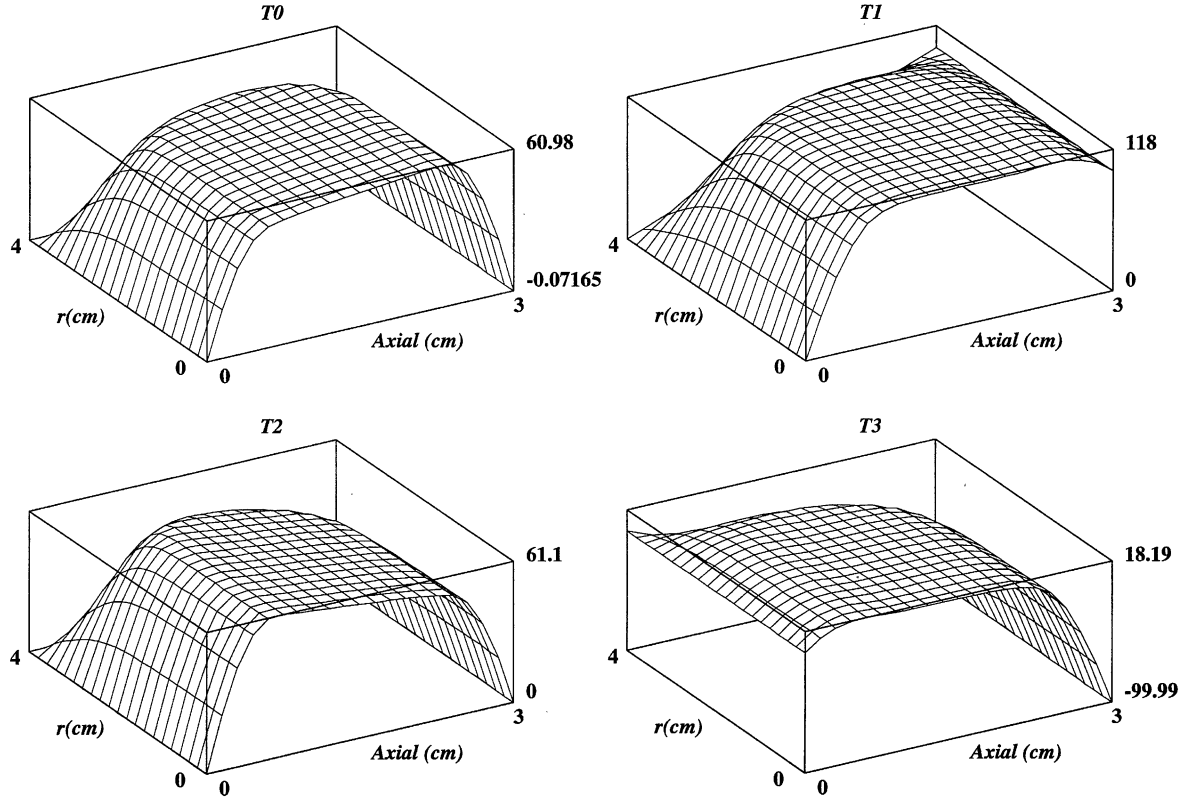

(b)

Fig. 3. (a) Ionization rate (10^{18}/cm^3 s) and (b) potential (V) profiles at four different times of an rf cycle. $V_{\rm rf} = 100$ V, $f = 10$ MHz, $p = 0.05$ Torr.

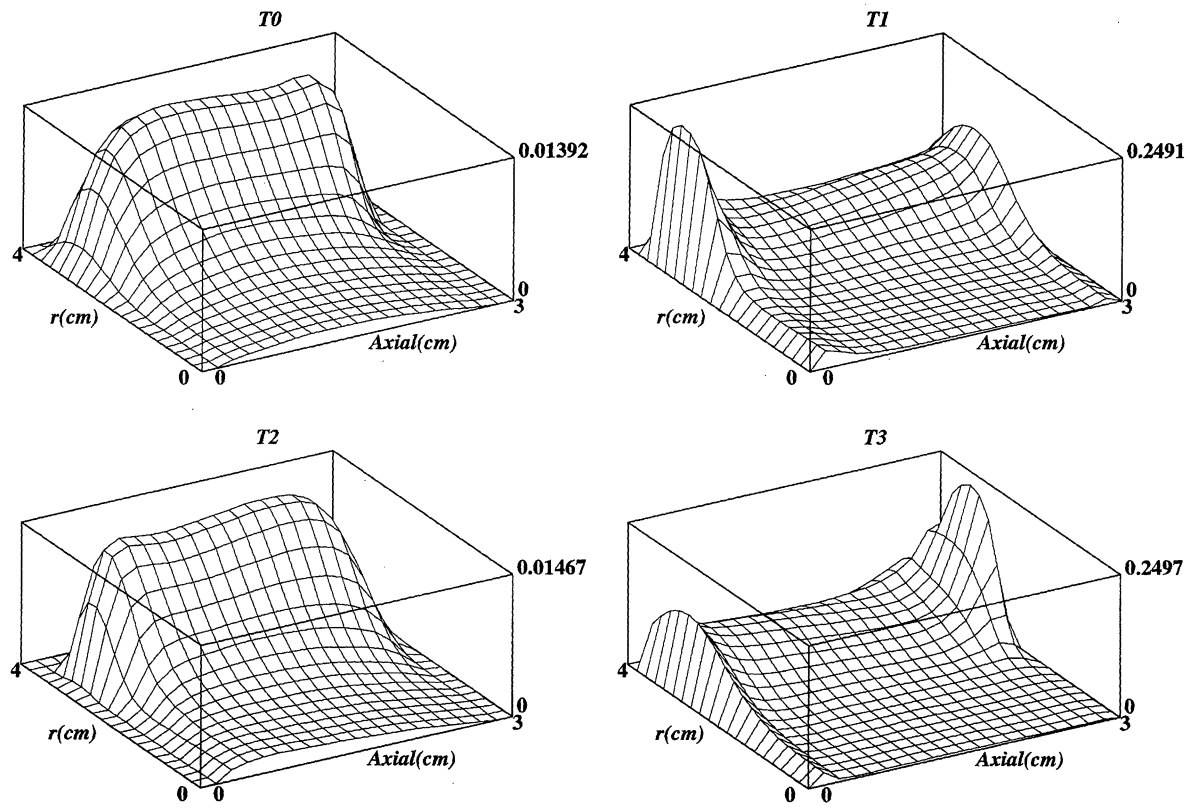

(a)

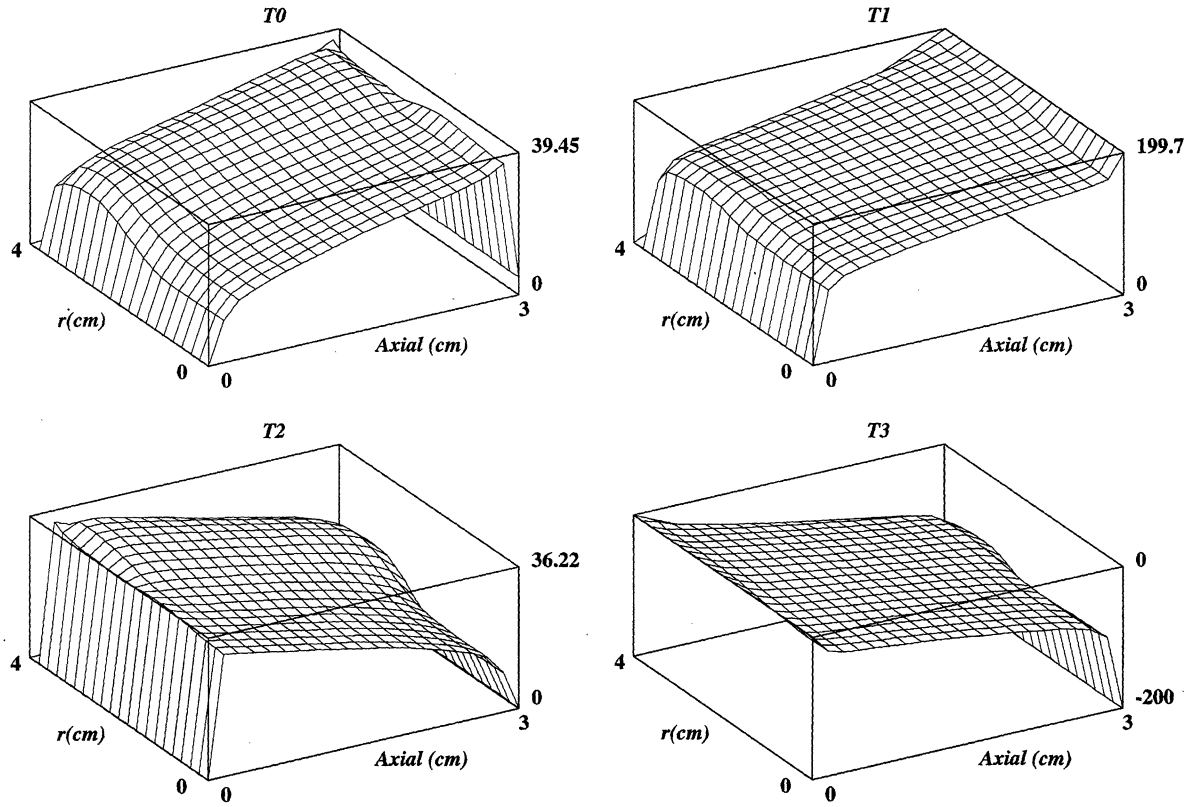

(b)

Fig. 4. (a) Ionization rate (10^{18}/cm^3 s) and (b) potential (V) profiles at four different times of an rf cycle. $V_{\mathrm{rf}} = 200$ V, $f = 10$ MHz, $p = 0.5$ Torr.

note is that the electron density is higher near the radial sheath region than the central region. This can be accounted for as follows: from the temperature profile, one observes that the electrons have a higher energy in the radial sheath region and in the vicinity of the boundary between the bulk and the radial sheath. Electrons in the radial sheath region are heated by the oscillating radial electric fields and provide a source of ionization. Electrons are involved in collisions when high-energy electrons move toward the bulk from the radial wall of the reactor and create a great number of ionization collisions in the sheath region.[15] The presence of high-energy electrons in the radial sheath region results in a markedly high ionization frequency.

When the rf frequency is increased to 100 MHz as shown in Fig. 5, the plasma potential increases by a small amount. The electron temperature decreases overall, but exhibits a spatial distribution similar to that before. The ionization rate is almost uniform in the bulk and has two slight peaks near the plasma-sheath boundary. The charged particle densities are increased by one order of magnitude compared to these in the $f = 10\,\mathrm{MHz}$ case.

From Fig. 6(a), we can note that the negative ion profile is parabolic at a neutral gas pressure of less than 100 mTorr, in agreement with theoretical and experimental results.[18,19] As the pressure is increased, flatter profiles are observed (Fig. 6(b)).

The average electron density, negative ion density, and plasma potential are calculated as a function of the gas pressure. The negative ion density is about 40 times

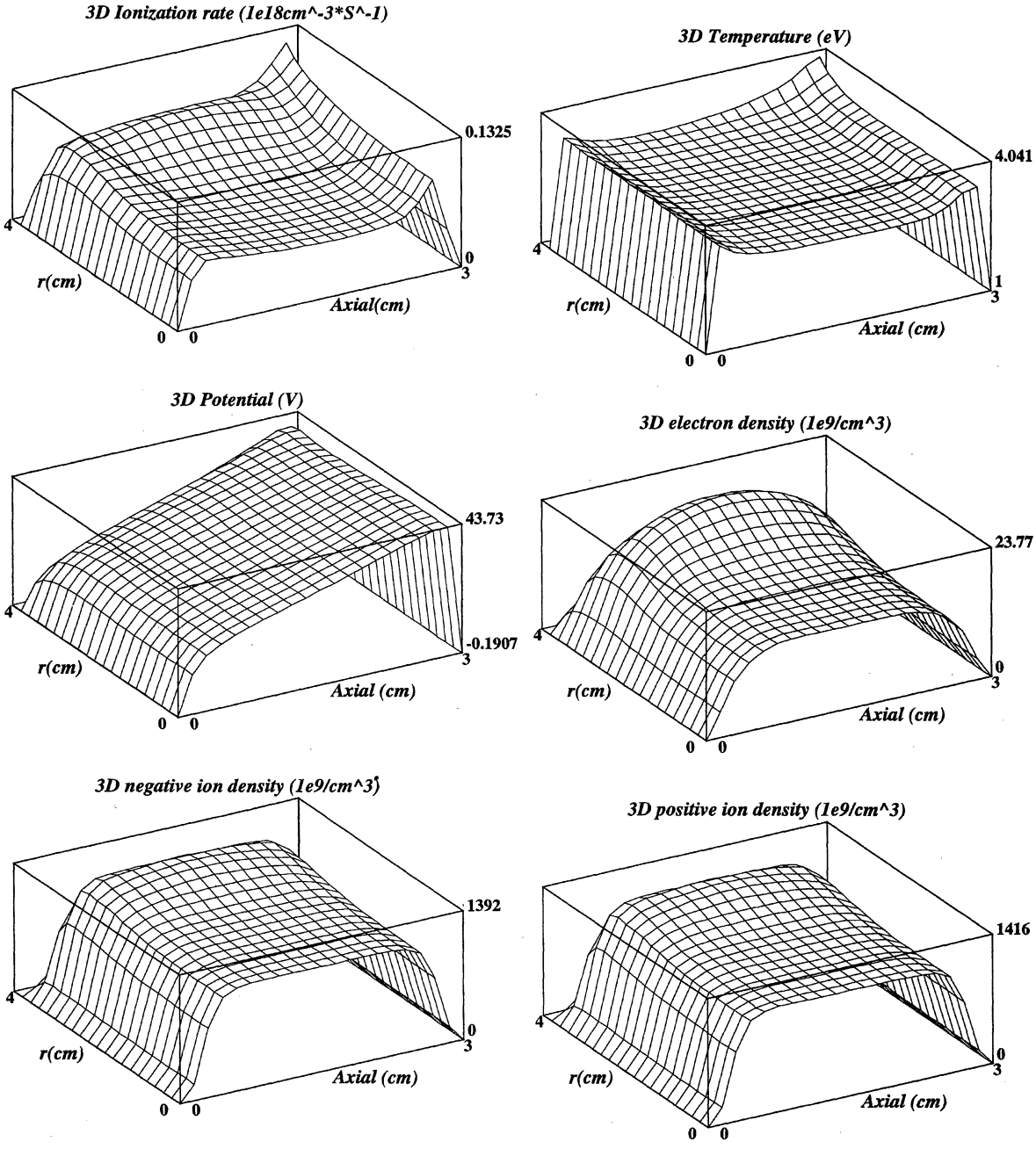

Fig. 5. The profiles of ionization rate, electron temperature, potential, electron density, negative ion density, and positive ion density at T_0 where $V_{\mathrm{rf}} = 150\,\mathrm{V}$, $p = 0.5\,\mathrm{Torr}$, and $f = 100\,\mathrm{MHz}$.

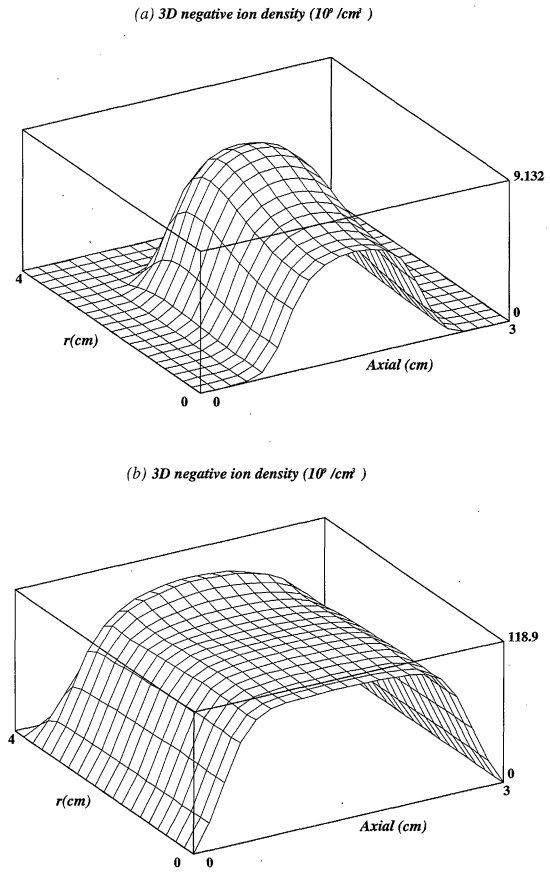

Fig. 6. Negative ion density profiles in a unit of 10^9 cm^{-3} for two pressures, (a) $p = 0.08$ Torr, and (b) $p = 0.7$ Torr.

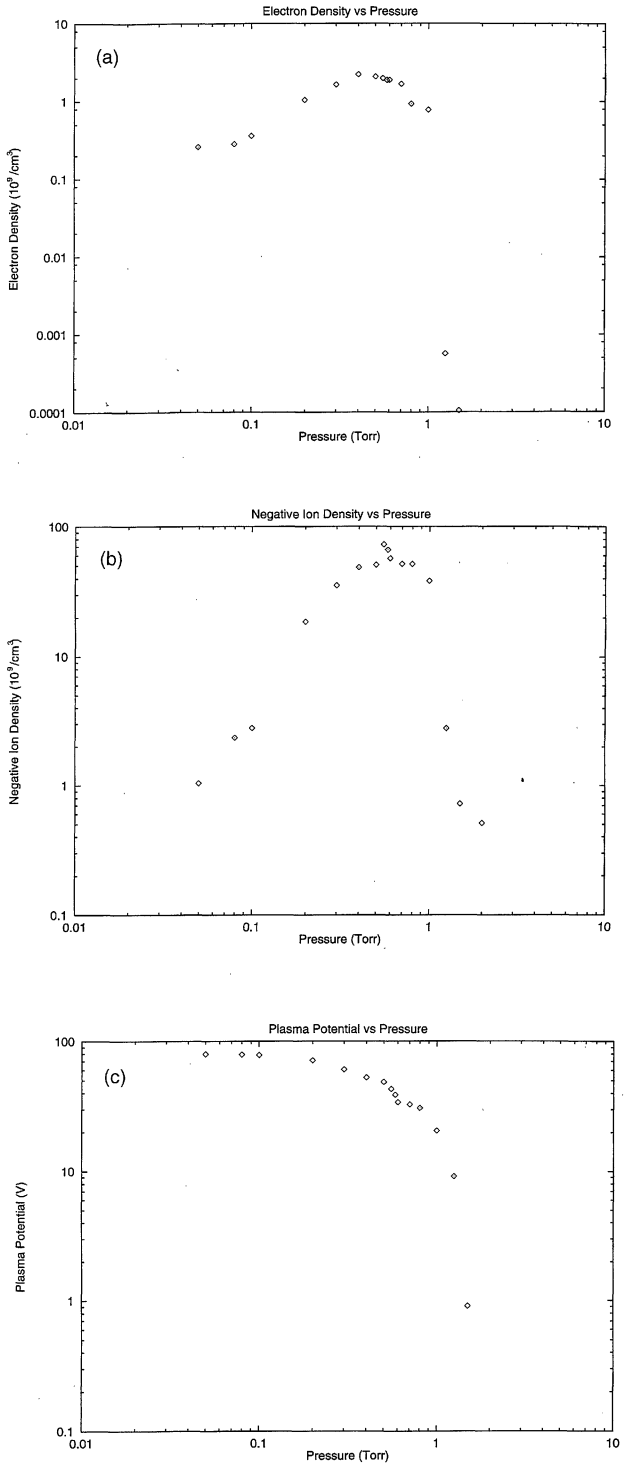

Fig. 7. (a) Average electron density vs pressure. (b) Average negative ion density vs pressure. (c) Plasma potential vs pressure. Here, $V_{\rm rf} = 150$ V and $f = 10$ MHz.

higher than the electron density in this operating region. The pressure dependences of the electron density, negative ion density, and plasma potential are shown in Figs. 7(a), 7(b), and 7(c). We can note that the decrease in the negative ion density with increasing pressure is pronounced. In a sophisticated model[19] in which various reactions involving cl neutrals are considered, the situation is more complicated. However, in this simple reaction model in which cl neutral reactions are neglected, cl^- balance is governed by dissociative attachment to cl_2 and ion–ion recombination, which causes its density to increase as the square root of pressure at low pressure, and to decrease rapidly at high pressure. Actually, this simple reaction model is meaningless above 1 Torr. Also it should be noted that in the formulation of this simulation, a low degree of dissociation and abundance of cl_2 ions, which is attributed to the ready recombination of cl atoms on the chamber walls, are assumed.

Figure 7(c) shows the plasma potential as a function of the gas pressure. As is well known, the plasma potential is proportional to the electron temperature. Therefore, the plasma potential decreases with the pressure. Shindo and Horiike showed that the floating potential with respect to the plasma potential (which is assumed to be zero) decreases with an increase in the negative ion concentration.[20] In this simulation, the plasma potential with respect to the ground (cathode potential) exhibits a sudden decrease in a region of high negative ion concentration.

4. Conclusions

Capacitively coupled rf discharges were simulated based on a two-dimensional fluid model. The two-dimensional distributions of charged particle densities, potential, electron temperature, and ionization rate were calculated. The results are in good qualitative agreement with the results of the most recent experimental investigations of the field and charge distribution. The effects of the applied rf voltage, the driver frequency, and the

gas pressure on the 2D profiles of the plasma properties such as the charged particle density, ionization rate, and potential were investigated. For a high rf voltage, the ionization peaks strongly in the radial sheath region, where the electric field strength and electron flux are largest. The average electron density, negative ion density, and plasma potential were calculated as a function of the gas pressure. The negative ion density is about 40 times higher than the electron density in this operating region.

Acknowledgements

This work was supported in part by Dong-A University, Korea Science and Engineering Foundation (Contract No. 951-0201-025-2), and the Basic Science Research Institute Program, Korea Ministry of Education (BSRI-95-2439).

1) D. B. Graves: IEEE Trans. Plasma Sci. **22** (1994) 31.
2) J. P. Boeuf and L. C. Pitchford: IEEE Trans. Plasma Sci. **19** (1991) 286.
3) J. P. Boeuf: J. Appl. Phys. **63** (1988) 1342.
4) J. P. Boeuf: Phys. Rev. A **36** (1987) 2782.
5) J. H. Tsai and C. Wu: Phys. Rev. A **41** (1990) 5626.
6) D. B. Graves and K. F. Jensen: IEEE Trans. Plasma Sci. **14** (1986) 78.
7) D. B. Graves: J. Appl. Phys. **62** (1987) 88.
8) S. K. Park and D. J. Economou: J. Appl. Phys. **68** (1990) 4888.
9) S. K. Park and D. J. Economou: J. Appl. Phys. **68** (1990) 3904.
10) A. D. Richards, B. E. Thompson and H. H. Sawin: Appl. Phys. Lett. **50** (1987) 492.
11) J. D. P. Passchier and W. J. Goedheer: J. Appl. Phys. **74** (1993) 3744.
12) V. Vahedi, P. Mirrashidi, D. K. Wong and J. Verboncoeur: Xgrafix (ver. 2.01), © Copyright 1991–1995 The Regents of the University of California.
13) J. K. Lee, L. Meng, Y. K. Shin, H. J. Lee and T. H. Chung: submitted to J. Appl. Phys. (1996).
14) E. Meeks and J. W. Shon: IEEE Trans. Plasma Sci. **23** (1995) 539.
15) F. F. Young and C. J. Wu: IEEE Trans. Plasma Sci. **21** (1993) 312.
16) D. L. Sharfetter and H. K. Gummel: IEEE Trans. Electron Devices **16** (1969) 64.
17) L. Meng, T. H. Chung and J. K. Lee: submitted to J. Appl. Phys. (1996).
18) D. Vender, W. W. Stoffels, E. Stoffels, G. M. W. Kroesen and F. J. de Hoog: Phys. Rev. E **51** (1995) 2436.
19) E. Stoffels, W. W. Stoffels, D. Vender, M. Kando, G. M. W. Kroesen and F. J. de Hoog: Phys. Rev. E **51** (1995) 2425.
20) H. Shindo and Y. Horiike: Jpn. J. Appl. Phys. **30** (1991) 161.